Convection Enhanced Delivery of Anti-angiogenic and Cytotoxic Agents in Combination Therapy against Brain Tumour

Dr. Wenbo Zhan

PII: S0928-0987(19)30367-7
DOI: https://doi.org/10.1016/j.ejps.2019.105094
Reference: PHASCI 105094

To appear in: *European Journal of Pharmaceutical Sciences*

Received date: 25 April 2019
Revised date: 22 August 2019
Accepted date: 28 September 2019

Please cite this article as: Dr. Wenbo Zhan , Convection Enhanced Delivery of Anti-angiogenic and Cytotoxic Agents in Combination Therapy against Brain Tumour, *European Journal of Pharmaceutical Sciences* (2019), doi: https://doi.org/10.1016/j.ejps.2019.105094

Convection Enhanced Delivery of Anti-angiogenic and Cytotoxic Agents in Combination Therapy against Brain Tumour

Dr. Wenbo Zhan[a,b,*] w.zhan@imperial.ac.uk

[a]School of Engineering, University of Aberdeen, Aberdeen, United Kingdom

[b]Department of Mechanical Engineering, Imperial College London, South Kensington Campus, London, United Kingdom

[*]Correspondence: Phone: +447706636021 ,+44(0)2075895111.

Abstract

Convection enhanced delivery is an effective alternative to routine delivery methods to overcome the blood brain barrier. However, its treatment efficacy remains disappointing in clinic owing to the rapid drug elimination in tumour tissue. In this study, multiphysics modelling is employed to investigate the combination delivery of anti-angiogenic and cytotoxic drugs from the perspective of intratumoural transport. Simulations are based on a 3-D realistic brain tumour model that is reconstructed from patient magnetic resonance images. The tumour microvasculature is targeted by *bevacizumab*, and six cytotoxic drugs are included, as *doxorubicin*, *carmustine*, *cisplatin*, *fluorouracil*, *methotrexate and paclitaxel*. The treatment efficacy is evaluated in terms of the distribution volume where the drug concentration is above the corresponding LD90. Results demonstrate that the infusion of *bevacizumab* can slightly improve interstitial fluid flow, but is significantly efficient in reducing the fluid loss from the blood circulatory system to inhibit the concentration dilution. As the transport of *bevacizumab* is dominated by convection, its spatial distribution and anti-angiogenic effectiveness present high sensitivity to the directional interstitial fluid flow. Infusing *bevacizumab* could enhance the delivery outcomes of all the six drugs, however, the degree of enhancement differs. The delivery of *doxorubicin* can be improved most, whereas, the impacts on *methotrexate and paclitaxel* are limited. *Fluorouracil* could cover the comparable distribution volume as *paclitaxel* in the combination therapy for effective cell killing. Results obtain in this study could be a guide for the design of this co-delivery treatment.

Graphical Abstract

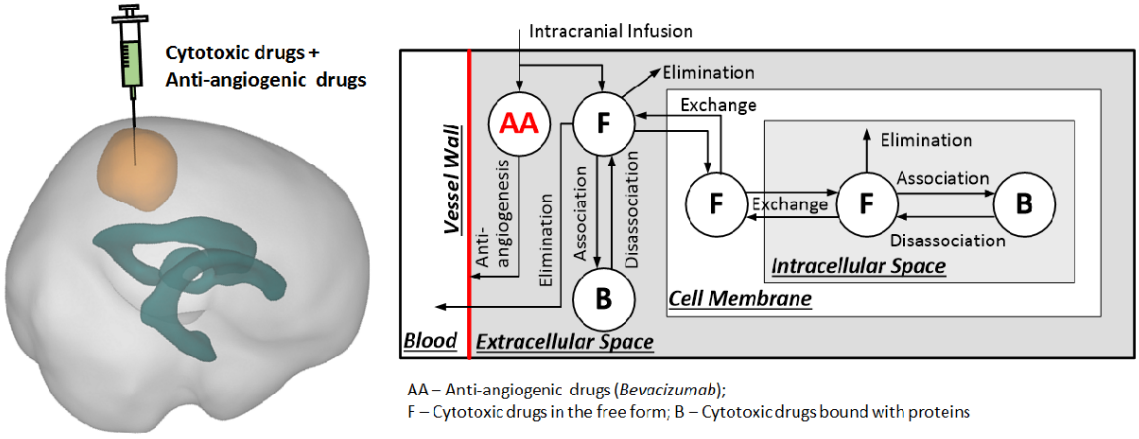

Keywords:

Anti-angiogenesis; Brain tumour; Convection enhanced delivery; Drug transport; Mathematical modelling

Introduction

Convection enhanced delivery (CED) is a promising alternative to intravenous administration for localised drug delivery against glioblastoma [1, 2]. As anticancer agents are directly infused into the lesion [3], the risk of adverse effects in chemotherapy can be largely reduced. However, the drug penetration and bioavailability remain disappointing in clinic [4], due to the rapid drug elimination in tumour tissue. Given that the microvasculature becomes elongated, tortuous and highly leakage in solid tumours [5, 6], the drug loss to blood circulatory system could significantly contribute to this efficient elimination.

Anti-angiogenetic therapy normalises the intratumoural vasculature by means of pruning vessels, remodelling and/or blocking angiogenesis, *etc*. Clinical trials have demonstrated the feasibility of anti-angiogenetic agents in combination with chemotherapy to improve the anticancer treatment [7]; these agents include *cedirani* [8, 9], *sunitinib* [10] and *bevacizumab* [11-14], *etc*. However, the effects of vascular normalisation may require for hours to days to

take place, raising a crucial challenge in the establishment of optimal timing for the combination [15], especially for the chemotherapy relying on intravenous administration that is performed within few hours. On the contrary, the continuous infusion in CED treatments usually last for serval days in clinic [1, 4, 16], enabling the concurrent administration of anti-angiogenic and cytotoxic agents. The combination of *bevacizumab* with CED has been studied in animal experiments [17], and the results demonstrated that this combination could prolong the animal survival.

Numbers of cytotoxic drugs have been developed with different mechanisms of action against cancer. *Cisplatin* [18], *carmustine* [19] and *doxorubicin* [20] inhibit the DNA replication by forming crosslinks in DNA or inhibiting biosynthesis of relative enzymes, while *paclitaxel* could result in defects in mitotic spindle assembly and cell division [21, 22]. To be different, *fluorouracil* [23] and *methotrexate* [24] kill cancer cells by inhibiting thymidylate synthase or the synthesis of thymidylates and proteins, *etc*. Although these drugs have been applied in clinical trials to treat brain cancer [25-32], there is a lack of understanding of how the anti-angiogenetic therapy influence their intratumoural transport. Since the outcomes of drug delivery are strongly dependent on the interplays between the biological systems and anticancer drugs [33], CED treatments could be benefited by examining the performances of different drugs in the combination therapy with anti-angiogenesis.

Computational modelling has become an indispensable approach in the study of drug delivery, because the cross-linked drug transport processes can be examined either individually or in an integrated manner. The modelling platform was established to examine the effects of different tumour properties on the delivery of antibodies in a series of pioneering work [34-36]. As the development for CED, this platform was fine-tuned to simulate the pressure-driven flow under infusion [37], and was applied to optimise different drug delivery systems and treatment regimens [38, 39] in order to improve the CED effectiveness. On the other

hand, the transport of *bevacizumab* [40] was included into the platform to predict the treatment efficacy of anti-angiogenesis under different intravenous administration protocols [41].

This study is aimed to examine the performances of different cytotoxic drugs in the combination treatments of CED with anti-angiogenesis under the same treatment regimen and delivery conditions. A multiphysics model is adopted to describe the key transport processes, including diffusive and convective transport in interstitial fluid, drug binding with proteins, association with cell membrane, cell uptake, and elimination due to blood drainage, enzymatic and non-enzymatic reactions. The model is applied to a 3-D realistic brain tumour model that is reconstructed from patient magnetic resonance (MR) images. The anti-angiogenic effect is induced by *bevacizumab*, and six cytotoxic drugs are examined, including *fluorouracil*, *carmustine*, *cisplatin*, *methotrexate*, *doxorubicin* and *paclitaxel*. Treatment efficacy is evaluated by the tissue volume where the drug concentration is greater than its corresponding LD90.

1. Methods and Materials

1.1. Mathematical model

Microvasculature network is capable of varying considerably in tumours regarding to the location and tumour growth stage [42]. Given the inter-capillary distance is generally 2~3 orders lower than the transport scale in tissue, the tumour and its surrounding tissue are usually treated as porous media, in which the microvasculature functions are described as distributed source terms [34]. Therefore, the mass and momentum conservation equations can be employed to predict the flow of Newtonian, incompressible interstitial fluid in the form of

$$\begin{aligned} \nabla \cdot \mathbf{v} &= F_{\mathrm{L}} \\ \rho(\mathbf{v} \cdot \nabla \mathbf{v}) &= -\nabla p_{\mathrm{i}} + \mu \nabla^2 \mathbf{v} - \left(\frac{\mu}{\kappa}\right) \mathbf{v} \end{aligned} \tag{1}$$

where p_i and **v** stand for the pressure and velocity of interstitial fluid. ρ and μ are the interstitial fluid density and viscosity, respectively. κ refers to the tissue Darcian permeability, which depends on the tissue type and microstructure, *etc*. F_L is the flux of fluid gain from the blood circulatory system, driven by the pressure gradient across the vessel wall.

$$F_L = K_b \varphi \frac{S}{V}[p_b - p_i - \sigma_T(\pi_b - \pi_i)] \quad (2)$$

in which K_b is the hydraulic conductivity of blood vessel wall. S/V stands for the microvasculature density, which is defined as the area of blood vessel wall per tissue volume. p_b is the blood pressure in the microvasculature lumen. φ is the variation scale of microvasculature density resulted by *bevacizumab*. π_b and π_i are the osmotic pressure in blood and interstitial fluid, respectively, and σ_T is the osmotic reflection coefficient.

The tumour and its holding brain tissue can briefly be divided into three compartments as the extracellular space (ECS), cell membrane (CM) and intracellular space (ICS). The processes of drug transport after infusion are schematically illustrated in **Figure 1**. The bioavailability of cytotoxic drugs are governed by the mass conservation equations, as

$$\begin{aligned} C_F &= v_{ECS}C_{F,ECS} + v_{CM}C_{F,CM} + v_{ICS}C_{F,ICS} \\ C_B &= v_{ECS}C_{B,ECS} + v_{CM}C_{B,CM} + v_{ICS}C_{B,ICS} \end{aligned} \quad (3)$$

where C represents the drug concentration, and v is the volume fraction of each tissue compartment. The subscript F and B refer to the free drugs and the drugs in their binding form with proteins, respectively. It is assumed that there is no drug either binding with proteins or being eliminated on cell membrane [43].

The concentration of free drugs in tissue (C_F) is governed by convective and diffusive transport in the interstitial fluid, loss to the blood circulatory system, cell uptake, elimination due to the physical degradation and metabolic reactions, as well as the association with proteins.

$$\frac{\partial C_{\mathrm{F}}}{\partial \mathrm{t}} = \upsilon_{\mathrm{ECS}} D_{\mathrm{F,ECS}} \nabla^2 C_{\mathrm{F,ECS}} - \nabla \cdot \left(\upsilon_{\mathrm{ECS}} C_{\mathrm{F,ECS}} \mathbf{v}\right) - \upsilon_{\mathrm{ECS}} (k_{\mathrm{b}} + k_{\mathrm{e}}) C_{\mathrm{F,ECS}} - \upsilon_{\mathrm{ICS}} k_{\mathrm{e}} C_{\mathrm{F,ICS}} - \frac{\partial C_{\mathrm{B}}}{\partial t} \quad (4)$$

where $D_{\mathrm{F,ECS}}$ is the drug diffusivity in tissue ECS. k_{e} is the elimination rate owing to the physical degradation and metabolism. $k_{\mathrm{b}} = \varphi PS/V$ stands for the drug loss rate to the blood circulatory system, in which P is the drug transvascular permeability. By introducing the assumptions [44] of (1) the linear correlations between free and bound drugs [45] ($K_{\mathrm{ECS}} = C_{\mathrm{B,ECS}}/C_{\mathrm{F,ECS}}$; $K_{\mathrm{ICS}} = C_{\mathrm{B,ICS}}/C_{\mathrm{F,ICS}}$) and (2) the equilibrium of free drug concentration reached among tissue compartments [46] ($P_{\mathrm{ICS-ECS}} = C_{\mathrm{F,ICS}}/C_{\mathrm{F,ECS}}$; $P_{\mathrm{CM-ECS}} = C_{\mathrm{F,CM}}/C_{\mathrm{F,ECS}}$), **Eq.(4)** can be simplified as

$$\frac{\partial C_{\mathrm{F,ECS}}}{\partial t} = D^*_{\mathrm{F,ECS}} \nabla^2 C_{\mathrm{F,ECS}} - \mathbf{v}^* C_{\mathrm{F,ECS}} - k^* C_{\mathrm{F,ECS}} \quad (5)$$

where $D^*_{\mathrm{F,ECS}} = (\upsilon_{\mathrm{ECS}}/\omega) D_{\mathrm{F,ECS}}$ is the apparent drug diffusivity, $\mathbf{v}^* = (\upsilon_{\mathrm{ECS}}/\omega)\mathbf{v}$ is the apparent velocity. $k^* = [\upsilon_{\mathrm{ECS}} k_{\mathrm{b}} + (\upsilon_{\mathrm{ECS}} + \upsilon_{\mathrm{ICS}}) k_{\mathrm{e}} + F_{\mathrm{b}}]/\omega$ is the drug apparent elimination rate, and $\omega = \upsilon_{\mathrm{ECS}}(1 + K_{\mathrm{ECS}}) + \upsilon_{\mathrm{ICS}} P_{\mathrm{ICS-ECS}}(1 + K_{\mathrm{ICS}}) + (1 - \upsilon_{\mathrm{ECS}} - \upsilon_{\mathrm{ICS}}) P_{\mathrm{CM-ECS}}$ depends on the drug and tissue properties.

The bioavailability of *bevacizumab* in tissue ECS is determined by diffusion and convection in the interstitial fluid and elimination [47]

$$\frac{\partial C_{\mathrm{AA}}}{\partial t} = D_{\mathrm{AA,ECS}} C_{\mathrm{AA}} - \nabla \cdot (\mathbf{v} C_{\mathrm{AA}}) - k_{\mathrm{AA,e}} C_{\mathrm{AA}} \quad (6)$$

in which $D_{\mathrm{AA,ECS}}$ and $k_{\mathrm{AA,e}}$ are the *bevacizumab* diffusivity and elimination rate, respectively. The anti-angiogenetic effect induced by *bevacizumab* can be described by [40]

$$\frac{\partial \varphi}{\partial t} = \varphi(\alpha + \beta\varphi + \gamma\varphi^2) - \varphi k_{\mathrm{AK}} C_{\mathrm{AA}} \quad (7)$$

where φ is the variation scale of microvascular density, and k_{AK} is the anti-angiogenetic rate. α, β and γ are the parameters describing the nature angiogenesis of tissue.

1.2. Model geometry

3-D geometry of the brain tumour and its holding tissue are reconstructed from anonymous MR images. Each 1 mm thick image slice comprises 256 by 256 pixels, and the pixel dimension is 1 mm. These images were acquired in three orthogonal planes, and are available on the image database of TCIA under the Creative Commons Attribution 3.0 Unported License for scientific purposes [48, 49]. A representative slice is given in **Figure 2(A)**.

The brain tumour and ventricle are segmented from the brain normal tissue on each slice based on the local signal intensity. The smoothed surfaces of tumour, ventricle and brain tissue are used to generate the computational mesh, which consists of 4.6 million tetrahedral elements for the mesh-independent solutions. The 3-D model is shown in **Figure 2(B)**. The equivalent radius of brain tumour and its holding tissue are 1.8 cm and 6.9 cm, respectively.

1.3. Model parameters

Given the modelling time window is much shorter as compared to the growth rate of solid tumour, constant geometrical parameters and properties of tumour and drugs [41] are assumed in this study. Model parameters together with their sources are summarised in **Table 1** and **Table 2** for tumour/normal tissue, anti-angiogenetic and cytotoxic drugs, respectively. The anti-/angiogenesis related parameters are derived from experiments [47, 50]. The anti-angiogenetic and cytotoxic agents are infused simultaneously at the constant infusion rate 3.0 μL/min to avoid potential damages to the tissue [4, 16]. The effective therapy concentration [43] refers to the drug concentration for resulting death in 90% of the cell population as measured in *ex vivo* experiments.

1.4. Numerical methods

The governing equations are solved by means of computational fluid dynamics. The SIMPLEC algorithm is employed to correlate pressure with the velocity correction. The

temporal and spatial discretisation of each equation are obtained by employing the 2nd order implicit Euler scheme and the 2nd order UPWIND scheme, respectively. Modelling convergence is controlled by setting the residual tolerance as 1E-5. The variation scale (φ) is initialised as 1.0 based on the assumption that the microvasculature density reaches equilibrium at the start of treatment.

1.5. Boundary Conditions

The gauge pressure on ventricle and brain surface are specified as 1447.4 Pa [54] and 657.9 Pa [81], respectively, with no flux of drugs. The continuity condition of all variables are imposed on the interface between tumour and its holding tissue. The catheter wall is assumed to be rigid with no slip or drug flux, while the constant velocity and concentration are imposed on the catheter tip where the CED infusion takes place.

2. **Results**

2.1. Anti-angiogenic effectiveness

The enhanced bulk flow of interstitial fluid is crucial in determining the drug penetration and accumulation in CED. As the infused *bevacizumab* is targeted on the microvasculature network for normalisation, this tissue structure change might reshape the intratumoural hydraulic environment and alter the drug delivery results. The governing equations are solved in the entire brain, subject to the aforementioned boundary conditions and model parameters listed in **Table 1** and **Table 2**. Results in **Figure 3(A)** show that *bevacizumab* exhibits a highly heterogeneous spatial distribution. It is not surprising that the *bevacizumab* concentration achieves the peak at the infusion site and decreases radially towards the tumour periphery. However, the reduction rate varies largely in different directions. A sharp fall can be found in front of the catheter. On the contrary, the concentration decreases gradually along the catheter track to the brain surface, with a low concentration region formed at the catheter

back. Consequently, the microvascular density is significantly reduced in the regions where *bevacizumab* accumulates, as shown in **Figure 3(B)**.

In order to understand the transport mechanism of *bevacizumab* in tumour ECS, the Péclet number (Pe) is introduced to evaluate the contribution of convection and diffusion, defined as

$$\mathrm{Pe} = Rv/D \tag{8}$$

where R is the equivalent radius of brain tumour. v represents the spatial averaged IFV in the entire brain tumour, which is 4.5E-7 m/s. As indicated by Pe = 2.53E+3 that is orders higher than 1.0, the transport of *bevacizumab* is dominated by convection rather than diffusion in the entire tumour. Therefore, the flow field is expected to be essential to determine the distribution and bioavailability of *bevacizumab*, and the consequential anti-angiogenic effectiveness.

2.2. Interstitial fluid flow

Figure 4 represents the flow field in the entire brain with and without the administration of *bevacizumab*. Results show that in both the treatments, the interstitial fluid flows from the ventricle towards the brain surface, due to the driven force of original pressure gradient in brain. The CED infusion can accelerate the fluid flow around the infusion site, however, this flow eventually directs to the brain surface as indicated by the 3D streamline in **Figure 4**.

Quantitative comparisons on the interstitial fluid flow are given in **Figure 5**. Results show that in both the treatments, CED infusion is able to raise the interstitial fluid pressure (IFP) and velocity (IFV) around the infusion site. Infusing *bevacizumab* could reduce the IFP throughout the brain tumour from the infusion site to the surface; this finding consists with the findings from experiments [82]. Therefore, the IFV can be slightly increased, as indicated by **Figure 5(B-b)**. This finding suggests that the flow velocity is mainly determined by the infusion, but the introduction of anti-angiogenesis could also contribute to the enhancement

on the interstitial fluid flow.

To be different, fluid leakage from blood (FL) can be significantly reduced in the combination treatment because of the dispersed microvasculature. This reduction is able to prevent the drug concentration being diluted, so as to benefit the treatment efficacy by keeping the drug concentration enough high for cell killing. It is worth to note that the fluid leakage begin to restore 3 mm away from the infusion site, suggesting that this dilution inhibition is effective within the region around the infusion site.

2.3. Distribution of cytotoxic drugs

The spatial distributions of each anticancer drug are represented in **Figure 6**. Regardless the drug type, concentrations of all the drugs decrease radially from the infusion site to the brian surface. As such, their non-uniform spatial distributions are formed. Except *paclitaxel* and *methotrexate*, the rest drugs mainly concentrate around the catheter tip in the *bevacizumab*-free treatment. Comparsions demonstrate that the drug distribution of all the examined drugs can be improved by the infusion of *bevacizumab*, indicting the combination with anti-angiogenesis can improve the CED treatment.

The non-uniformity (NUN) of drug spatial distribution can be calculated in terms of the local and averaged concentration

$$\mathrm{NUN} = \frac{\sum |C_\mathrm{i} - C_\mathrm{avg}| V_\mathrm{i}}{C_\mathrm{avg} V_\mathrm{Tumour}} \tag{9}$$

where C_i and V_i are the local drug ECS concentration and corresponding local volume, respectively. C_avg is the spatial averaged drug concentration in tumour ECS, and V_Tumour refers to the volume of whole brain tumour. NUN reflects the spatial variation of drug concentration, with the higher value standing for the overall heterogeneous distribution. As compared in **Figure 7**, the infusion of *bevacizumab* is able to reduce the NUN values for all

the drugs. This finding denotes that the combination with anti-angiogenesis could homogenise the distribution of cytotoxic drug in the entire tumour to improve the CED therapy.

Given that each drug has different elimination rates and diffusivity in the tumour ECS, a dimensionless number, R_{IC}, can be introduced to examine the importance of convective transport in determining the drug spatial distribution. The definition is given below, and results are summarised in **Table 3**.

$$R_{IC} = \frac{v_s}{\sqrt{Dk}} \quad (10)$$

Comparisons demonstrate that infusion of *bevacizumab* is capable of raising R_{IC} for each of the cytotoxic drugs. Therefore, the convective transport becomes more important than diffusion and elimination in determining the drug transport in the combination therapy. Considering that the interstitial fluid flow can be slightly accelerated by anti-angiogenesis as shown in **Figure 5 (B-b)**, the cytotoxic drugs can reach the deep tumour tissue for more homogenised distribution.

2.4. Penetration of cytotoxic drugs

The effect of anti-angiogenesis on cytotoxic drug concentration are represented in **Figure 8** as a function of the distance from the infusion site. Results demonstrate that the infusion of *bevacizumab* is able to maintain the cytotoxic drug concentrations, and hence improve the drug penetration into brain tumour. However, this improvement is strongly dependent on the drug properties. Quantitative analyses show that the treatment using *doxorubicin* can be improved most. This is followed by *cisplatin*, *fluorouracil* and *carmustine*, whereas, the influences of anti-angiogenesis on the delivery of *paclitaxel* and *methotrexate* are less significant.

Since the infused *bevacizumab* mainly affect the microvascular-related elimination, incuding

blood drainage (k_{b}) and concentration dilution due to the fluid loss (F_{b}), a demensionless number of $\mathrm{R_{IB}}$ is introduced to evaluate the contribution of microvascular-related elimination as compared to the metabolic reactions and physical degradation, defined as

$$\mathrm{R_{IB}} = \frac{\upsilon_{\mathrm{ECS}} k_{\mathrm{b}} + F_{\mathrm{b}}}{(\upsilon_{\mathrm{ECS}} + \upsilon_{\mathrm{ICS}}) k_{\mathrm{e}}} \tag{11}$$

The lower value of $\mathrm{R_{IB}}$ indicates less importance of microvascular-related elimination in determining the cytotoxic drug clearance. As shown in **Table 4,** the infusion of *bevacizumab* could reduce the contribution of microvascular-related elimination for all the drugs. Since *doxorubicin* experiences the most elimination due to the presence of microvasculature, anti-angiogenesis is capable of significantly enhancing its penetration. On the contrary, *paclitaxel* and *methotrexate* present low sensitivity to anti-angiogenesis because their elimination are mainly determined by metabolism and physical degradation, which stay constantly in the combination therapy.

2.5. Accumulation of cytotoxic drugs

Achieving enough high drug concentration is essential to introduce effective cytotoxicity in cancer therapy. Given the drug intratumoural deposition varies with the location as shown in **Figure 6**, the spatial averaged concentration (C_{avg}) is applied to evaluate the drug accumulation in the entire tumour, defined as

$$C_{\mathrm{avg}} = \frac{\sum C_{\mathrm{i}} V_{\mathrm{i}}}{\sum V_{\mathrm{i}}} = \frac{\sum C_{\mathrm{i}} V_{\mathrm{i}}}{V_{\mathrm{Tumour}}} \tag{12}$$

Compared in **Figure 9** are the spatial averaged concentration of each cytotoxic drug in the *bevacizumab*-free CED and the combination therapy. Although the most effective drug accumulation are achieved by *paclitaxel* and *methotrexate* in both the treatments, anti-angiogenesis can largely increase the concentrations of the rest four drugs to the comparable levels. This consists with the findings of the heterogeneous drug distributions as shown in

Figure 7.

Given the drug diffusivity are not changed by the infusion of *bevacizumab*, the drug bioavailability can be evaluated in terms of the Karlovitz number (Ka) which is defined as

$$\mathrm{Ka} = \frac{v_s}{Rk} \tag{13}$$

As shown in **Table 5**, the time scale of convective transport is smaller than that of elimination for all the drugs. However, higher values of Ka indicate that the delivery of *paclitaxel* and *methotrexate* are less determined by elimination as compared to the rest four drugs. As such, *paclitaxel* and *methotrexate* could reach relatively higher concentration. On the contrary, the rest four drugs could be eliminated before transporting into deep brain tissue with the interstitial fluid flow. Although anti-angiogenesis can reduce the elimination for *doxorubicin*, *cisplatin*, *fluorouracil* and *carmustine*, their delivery are still dominated by elimination. So that their accumulation remain less effective as compared to *paclitaxel* and *methotrexate*.

2.6. Cytotoxic effectiveness

It is important to note that, rather than linearly correlating to the concentration, the cytotoxic effectiveness for different drugs are also determined by their unique pharmacodynamics process. To this end, instead of the averaged drug concentration (C_{avg}), the cytotoxic effectiveness is evaluated in terms of the tissue volume (V_{eff}) in which the drug concentration ($C_{\mathrm{F,ECS}}$) is enough high to kill 90% of the cell population as measured in *ex vivo* experiments (LD90).

$$V_{\mathrm{eff}} = \sum V_i \quad \left(C_{\mathrm{F,ECS}} \geq \mathrm{LD90}\right) \tag{14}$$

Results in **Figure 10** show that the infusion of *bevacizumab* can enlarge the effective distribution volume for better treatment efficacy. *Paclitaxel* is found as the most effective

drug in *bevacizumab*-free treatment. However, enhanced by the *bevacizumab*-induced reduction in microvasculature density, *fluorouracil* is able to cover comparable tumour volume for effective cell killing in the combination therapy.

3. **Discussion**

CED improves the delivery outcomes by facilitating a friendly hydraulic environment for drug transport. The infusion is able to build up the interstitial fluid pressure around the infusion site. On the one hand, this raised pressure can accelerate the bulk flow of interstitial fluid, and thereby improve the drug convective transport for better penetration. On the other hand, the decreased transvascular pressure gradient reduces the fluid loss from blood, so that the drug concentration dilution can be inhibited. The co-delivery with *bevacizumab* presents its superiority in further reducing the fluid loss, which is beneficial to maintain the drug concentration enough high for effective cytotoxicity. Moreover, *bevacizumab* can slightly accelerate the interstitial fluid flow, further improve the penetration of cytotoxic drugs.

The movement of *bevacizumab* in brain tumour ECS mainly relies on the convective transport. Worth to note that this convection is dominated by CED infusion around the infusion site, whereas, in the rest tumour region the directional interstitial fluid flow from brain ventricle to arachnoid plays a crucial role. This transport mechanism of *bevacizumab*, in turn, requires the infusion catheter to be placed with respect to the flow field in the entire brain. Catheter pose and infusion orientation should be carefully designed to avoid possible ineffective delivery, as the low *bevacizumab* concentration region at the catheter back shown in **Figure 3**.

Drugs behave differently in response to anti-angiogenesis. *Doxorubicin* presents the most limited bioavailability in the control study without *bevacizumab*, due to the rapid blood drainage that can quickly move the drugs out of tumour ECS. As a consequence, the

reduction of microvasculature density can effectively maintain *doxorubicin* concentration, and thereby enhance the delivery outcomes. On the contrary, *methotrexate* and *paclitaxel* experience less elimination and are able to transport with the interstitial fluid flow into the deep tumour region. Although the blood drainage is also inhibited, anti-angiogenesis has little contribution to the delivery of these two drugs. Given intratumoural drug delivery are determined by the interplays between the biological systems and drugs, findings from this study could provide suggestions to the choice of drugs in this combination therapy.

Anti-angiogenetic agents are mainly delivered by systemic administration in clinical trials. Through daily oral administration, *cediranib* was capable of opening a time window (> 4-week) of vascular normalisation in recurrent glioblastomas [15], enabling the combination with chemotherapy to enhance the treatment efficacy [9]. Intravenous *bevacizumab* has been shown to successfully reduce 29~59% microvascular density in renal cancers by 12 days [82]. However, its applications alone or with *irinotecan* could be less effective in the treatments against recurrent and newly diagnosed brain tumours [83, 84]. As an alternative, *bevacizumab* was continuously infused into the tumours for 28 days via CED. Compared to the animals treated with intravenous *bevacizumab*, the prolonged animal survival demonstrated the feasibility of CED *bevacizumab* for treating brain tumours either alone or in the combination with chemotherapy [17]. It is also worth to point out that, apart from intravenous administration which is carried out within few hours, the infusion in CED treatments usually lasts over days or weeks in clinical trials [1, 4, 16, 85, 86]. This continuous infusion could also benefit the anti-angiogenetic therapy which may require for days to play the role. As there is a lack of clinical trials using CED *bevacizumab*, *bevacizumab* and cytotoxic drugs are idealised infused simultaneously into the brain tumour in this study. Future studies are required to optimise the timing for the infusion of anti-angiogenic and cytotoxic drugs.

The insertion of catheter into brain is possible to cause tissue trauma and thereby leads to edema. The excess fluid due to the enhanced leakage from circulatory system could result in tissue swelling and backflow around the infusion catheter. These changes in hydraulic environment, as the main limitations in CED, might affect the drug intratumoural transport and accumulation. On the other hand, clinical trials have shown that anti-angiogenetic agents could alleviate the vasogenic edema [15], so as to ease those limitations. Since there is limited mathematical models that can descript the formation of edema in CED treatment or how anti-angiogenetic agents inhibit edema, this process in the combination therapy has yet been included in the present study. The corresponding mathematical model could be developed with supports from experimental measurements in the future.

The mathematical model is applied to evaluate the performances of different cytotoxic drugs in the combination CED treatment with anti-angiogenetic agents under the same delivery conditions. As drug delivery incorporate series of biological and physicochemical processes, several factors could affect the treatment efficacy; these factors include the transport properties of drugs, biological properties of tumour and administration protocols. Comprehensive parameter study can be performed to identify the impacts and importance of each factor for optimisation [87, 88]. This study could be more applicable for nanocarriers as their properties could be tailored by modifying the formulation, morphology and fabrication process, *etc.* [89-92], whereas, the properties of small molecular drugs mainly depend on their intrinsic formula. One should note that the model also needs to be further developed to describe the certain process [39], such as the release of free drugs from nanocarriers.

The delivery outcomes predicted by mathematical modelling agree well with experimental data under the same delivery conditions [38, 93] as shown in **Figure 11**. The mathematical model of drug delivery has been validated in several studies. The original model predicted the interstitial fluid velocity as 0.17 μm/s [34], which was in the range of 0.13~0.2 μm/s as

obtained from experiments [95]. The same model has been applied in a realistic tumour model [71], and the predicted interstitial fluid pressure of 1500 Pa and 40 Pa well located in the measured ranges of 587~4200 Pa and -400~800 Pa for solid tumours and the holding tissue, respectively [37]. As indicated by the coefficients of multiple determination (R^2) of 0.8 and 0.7, good agreements have been achieved between the simulations and experiments of the convection enhanced delivery of Evans Blue and albumin into gel, respectively [96]. However, it is important to point out that the modelling predictions remain qualitative when comparing to *in vivo* experiments [43]. This could be attributed to the lack of mathematical descriptions for the complex biochemical processes and the inaccurate model parameters to present the realistic properties of the tumour and drugs. In summary, mathematical modelling could provide the qualitative trends of drug delivery results against the variations of examined factors. These predictions are capable of assisting in identifying the influence of different factors and offering opportunities to optimise the treatment regimens. Insight from biochemical studies and studies on the molecular level could help establish mathematical descriptions for particular drug delivery processes, and the application of medical images is a promising approach to determine the biological properties for model development.

This study is aimed to compare the performances of different cytotoxic drugs in the combination CED with anti-angiogenesis. Although some new insight can be provided, this study involves several assumptions and limitations. (1) The infusion catheter is idealised placed in the tumour centre. Given the importance of directional interstitial fluid flow to the transport of *bevacizumab*, the catheter pose and infusion direction need to be optimised in the future study. (2) The clinical CED usually lasts for several days [4, 16]. This time window could be sufficient for the drug accumulation and penetration to reach a quasi-steady state, at which the dynamic equilibrium is achieved between the source term of infusion and the sink term of elimination. Therefore, stationary simulations are carried out in this study to represent

411 the delivery outcomes at this quasi-steady state, corresponding to the potential maximum
412 efficacy that can be achieved. However, the treatment is a dynamic process which relates to
413 time, and its efficacy also depends on the clinical operations, including infusion duration,
414 infusion rate, and dosage, *etc*. Therefore, transient simulations can be performed to obtain the
415 temporal files of drug delivery outcomes, and following studies could also centre on the
416 infusion protocol and parameters for optimisation. (3) The spatial distribution of
417 microvasculature in solid tumour and the surrounding holding tissue can be heterogeneous,
418 especially in the large tumours or the tumours with necrotic core. This non-uniform
419 microvasculature could affect the drug transport and accumulation. However, because the
420 microvasculature information cannot be predicted from the available medical images, the
421 microvasculature is assumed to be uniformly distributed in the studied brain tumour [38, 43,
422 97]. Parameters adopted in this work correspond to the averaged and representative values
423 from literatures, as given in **Table 1** and **Table 2**. This assumption can be relaxed by using
424 dynamic contrast enhanced MR images [98, 99], on which the signal intensity correlates to
425 the concentration of imaging tracer. By applying the drug transvascular transport equation
426 [100], the microvascular density can be calculated from spatiotemporal profiles of the tracer.
427 (4) This study is focused on the drug transport. Apart from enhancing cytotoxicity, the anti-
428 angiogenic therapy could also reduce the supply of oxygen and nutrients to the solid tumour,
429 and thereby result in the cell death. To this end, the simulations can be further developed by
430 including the models for transport of oxygen and nutrients, cell signalling and cell life circle,
431 as well as pharmacodynamics in order to predict the spatiotemporal profiles of drug delivery
432 and cell killing in this combination therapy.

433 4. Conclusions

434 Convection enhanced delivery of anti-angiogenic and cytotoxic drugs into a brain tumour has
435 been studied based on a multiphysics model. Results demonstrate that anti-angiogenesis can

436 slightly enhance the bulk flow of interstitial fluid, but could significantly reduce the fluid loss
437 from the blood circulatory system. This reduction is beneficial to prevent the dilution of drug
438 concentration. The transport of *bevacizumab* is dominant by convection rather than diffusion
439 in the tumour extracellular space. Therefore, the directional interstitial fluid flow could play
440 an important role in determining its spatial distribution, and further influence the
441 effectiveness of anti-angiogenic therapy. Results show that infusing *bevacizumab* is able to
442 enhance the delivery outcomes of all the examined drugs, however, the responses to anti-
443 angiogenesis differ from drugs. The penetration and accumulation of *doxorubicin*, *cisplatin*,
444 *fluorouracil* and *carmustine* are more sensitive to the reduction in microvasculature density,
445 while the impact of anti-angiogenesis on the delivery of *paclitaxel* and *methotrexate* are
446 relatively limited. Results obtain in study could serve as a guide for this combination therapy
447 using CED.

448

449 **Competing interests**:

450 The author declares that there is no competing interests.

451 **References**

452 [1] A. Jahangiri, A.T. Chin, P.M. Flanigan, R. Chen, K. Bankiewicz, M.K. Aghi, Convection-
453 enhanced delivery in glioblastoma: a review of preclinical and clinical studies, Journal of
454 neurosurgery, 126 (2017) 191-200.

455 [2] G.D. Arnone, A.D. Bhimani, T. Aguilar, A.I. Mehta, Localized targeted antiangiogenic drug
456 delivery for glioblastoma, Journal of neuro-oncology, 137 (2018) 223-231.

457 [3] R.R. Lonser, M. Sarntinoranont, P.F. Morrison, E.H. Oldfield, Convection-enhanced delivery to
458 the central nervous system, Journal of neurosurgery, 122 (2015) 697-706.

459 [4] R. Raghavan, M.L. Brady, M.I. Rodríguez-Ponce, A. Hartlep, C. Pedain, J.H. Sampson,
460 Convection-enhanced delivery of therapeutics for brain disease, and its optimization, Neurosurgical
461 focus, 20 (2006) E12.

462 [5] M.R. Dreher, W. Liu, C.R. Michelich, M.W. Dewhirst, F. Yuan, A. Chilkoti, Tumor vascular
463 permeability, accumulation, and penetration of macromolecular drug carriers, Journal of the National
464 Cancer Institute, 98 (2006) 335-344.

465 [6] L.S. Heuser, F.N. Miller, Differential macromolecular leakage from the vasculature of tumors,
466 Cancer, 57 (1986) 461-464.

[7] N. Wang, R.K. Jain, T.T. Batchelor, New directions in anti-angiogenic therapy for glioblastoma, Neurotherapeutics, 14 (2017) 321-332.

[8] K.E. Emblem, K. Mouridsen, A. Bjornerud, C.T. Farrar, D. Jennings, R.J. Borra, P.Y. Wen, P. Ivy, T.T. Batchelor, B.R. Rosen, Vessel architectural imaging identifies cancer patient responders to anti-angiogenic therapy, Nature medicine, 19 (2013) 1178-1183.

[9] T.T. Batchelor, E.R. Gerstner, K.E. Emblem, D.G. Duda, J. Kalpathy-Cramer, M. Snuderl, M. Ancukiewicz, P. Polaskova, M.C. Pinho, D. Jennings, Improved tumor oxygenation and survival in glioblastoma patients who show increased blood perfusion after cediranib and chemoradiation, Proceedings of the national academy of sciences, 110 (2013) 19059-19064.

[10] I. Tamaskar, P. Shaheen, L. Wood, S. Hodnick, C. Nemec, J. Garcia, R. Dreicer, B. Rini, R. Bukowski, Antitumor effects of sorafenib and sunitinib in patients (pts) with metastatic renal cell carcinoma (mRCC) who had prior therapy with anti-angiogenic agents, Journal of Clinical Oncology, 24 (2006) 4597-4597.

[11] T. Shih, C. Lindley, Bevacizumab: an angiogenesis inhibitor for the treatment of solid malignancies, Clinical therapeutics, 28 (2006) 1779-1802.

[12] S. Kopetz, P.M. Hoff, J.S. Morris, R.A. Wolff, C. Eng, K.Y. Glover, R. Adinin, M.J. Overman, V. Valero, S. Wen, Phase II trial of infusional fluorouracil, irinotecan, and bevacizumab for metastatic colorectal cancer: efficacy and circulating angiogenic biomarkers associated with therapeutic resistance, Journal of clinical oncology, 28 (2010) 453-459.

[13] L.B. Saltz, S. Clarke, E. Díaz-Rubio, W. Scheithauer, A. Figer, R. Wong, S. Koski, M. Lichinitser, T.-S. Yang, F. Rivera, Bevacizumab in combination with oxaliplatin-based chemotherapy as first-line therapy in metastatic colorectal cancer: a randomized phase III study, Journal of clinical oncology, 26 (2008) 2013-2019.

[14] H.-P. Gerber, N. Ferrara, Pharmacology and pharmacodynamics of bevacizumab as monotherapy or in combination with cytotoxic therapy in preclinical studies, Cancer research, 65 (2005) 671-680.

[15] T.T. Batchelor, A.G. Sorensen, E. di Tomaso, W.-T. Zhang, D.G. Duda, K.S. Cohen, K.R. Kozak, D.P. Cahill, P.-J. Chen, M. Zhu, AZD2171, a pan-VEGF receptor tyrosine kinase inhibitor, normalizes tumor vasculature and alleviates edema in glioblastoma patients, Cancer cell, 11 (2007) 83-95.

[16] Y. Mardor, Y. Roth, Z. Lidar, T. Jonas, R. Pfeffer, S.E. Maier, M. Faibel, D. Nass, M. Hadani, A. Orenstein, Monitoring response to convection-enhanced taxol delivery in brain tumor patients using diffusion-weighted magnetic resonance imaging, Cancer research, 61 (2001) 4971-4973.

[17] W. Wang, W. Sivakumar, S. Torres, N. Jhaveri, V.P. Vaikari, A. Gong, A. Howard, E.B. Golden, S.G. Louie, A.H. Schönthal, Effects of convection-enhanced delivery of bevacizumab on survival of glioma-bearing animals, Neurosurgical focus, 38 (2015) E8.

[18] G. Chu, Cellular responses to cisplatin. The roles of DNA-binding proteins and DNA repair, Journal of Biological Chemistry, 269 (1994) 787-790.

[19] V. Beljanski, L.G. Marzilli, P.W. Doetsch, DNA damage-processing pathways involved in the eukaryotic cellular response to anticancer DNA cross-linking drugs, Molecular pharmacology, 65 (2004) 1496-1506.

[20] O. Tacar, P. Sriamornsak, C.R. Dass, Doxorubicin: an update on anticancer molecular action, toxicity and novel drug delivery systems, Journal of pharmacy and pharmacology, 65 (2013) 157-170.

[21] R. Bharadwaj, H. Yu, The spindle checkpoint, aneuploidy, and cancer, Oncogene, 23 (2004) 2016-2027.

[22] D.A. Brito, Z. Yang, C.L. Rieder, Microtubules do not promote mitotic slippage when the spindle assembly checkpoint cannot be satisfied, The Journal of cell biology, 182 (2008) 623-629.

[23] D.B. Longley, D.P. Harkin, P.G. Johnston, 5-fluorouracil: mechanisms of action and clinical strategies, Nature reviews cancer, 3 (2003) 330-338.

[24] P.R. Rajagopalan, Z. Zhang, L. McCourt, M. Dwyer, S.J. Benkovic, G.G. Hammes, Interaction of dihydrofolate reductase with methotrexate: ensemble and single-molecule kinetics, Proceedings of the National Academy of Sciences, 99 (2002) 13481-13486.

[25] V. Benitez, M.A. Karajannis, Chemotherapy of Brainstem Gliomas, in: Handbook of Brain Tumor Chemotherapy, Molecular Therapeutics, and Immunotherapy, Elsevier, 2018, 585-596.

[26] V. Levin, W. Hoffman, T. Pischer, M. Seager, E. Boldrey, C. Wilson, BCNU-5-fluorouracil combination therapy for recurrent malignant brain tumors, Cancer treatment reports, 62 (1978) 2071-2076.

[27] M.J. van den Bent, A.A. Brandes, R. Rampling, M.C. Kouwenhoven, J.M. Kros, A.F. Carpentier, P.M. Clement, M. Frenay, M. Campone, J.-F. Baurain, Randomized phase II trial of erlotinib versus temozolomide or carmustine in recurrent glioblastoma: EORTC brain tumor group study 26034, Journal of Clinical Oncology, 27 (2009) 1268-1274.

[28] A.B. Khan, B.J. D'Souza, M.D. Wharam, L. Champion, L.F. Sinks, S.Y. Woo, D.C. McCullough, B.G. Leventhal, Cisplatin therapy in recurrent childhood brain tumors, Cancer treatment reports, 66 (1982) 2013-2020.

[29] R.S. Dhanikula, A. Argaw, J.-F. Bouchard, P. Hildgen, Methotrexate loaded polyether-copolyester dendrimers for the treatment of gliomas: enhanced efficacy and intratumoral transport capability, Molecular Pharmaceutics, 5 (2008) 105-116.

[30] C.H. Tator, W. Wassenaar, Intraneoplastic injection of methotrexate for experimental brain-tumor chemotherapy, Journal of neurosurgery, 46 (1977) 165-174.

[31] K. Fabel, J. Dietrich, P. Hau, C. Wismeth, B. Winner, S. Przywara, A. Steinbrecher, W. Ullrich, U. Bogdahn, Long-term stabilization in patients with malignant glioma after treatment with liposomal doxorubicin, Cancer: Interdisciplinary International Journal of the American Cancer Society, 92 (2001) 1936-1942.

[32] Z. Lidar, Y. Mardor, T. Jonas, R. Pfeffer, M. Faibel, D. Nass, M. Hadani, Z. Ram, Convection-enhanced delivery of paclitaxel for the treatment of recurrent malignant glioma: a phase I/II clinical study, Journal of neurosurgery, 100 (2004) 472-479.

[33] W. Zhan, M. Alamer, X.Y. Xu, Computational modelling of drug delivery to solid tumour: Understanding the interplay between chemotherapeutics and biological system for optimised delivery system, Advanced Drug Delivery Reviews, (2018) 81-103.

[34] L.T. Baxter, R.K. Jain, Transport of fluid and macromolecules in tumors. I. Role of interstitial pressure and convection, Microvascular research, 37 (1989) 77-104.

[35] L.T. Baxter, R.K. Jain, Transport of fluid and macromolecules in tumors. II. Role of heterogeneous perfusion and lymphatics, Microvascular research, 40 (1990) 246-263.

[36] L.T. Baxter, R.K. Jain, Transport of fluid and macromolecules in tumors: III. Role of binding and metabolism, Microvascular research, 41 (1991) 5-23.

[37] S. Raghunathan, D. Evans, J.L. Sparks, Poroviscoelastic modeling of liver biomechanical response in unconfined compression, Annals of biomedical engineering, 38 (2010) 1789-1800.

[38] A.A. Linninger, M.R. Somayaji, M. Mekarski, L. Zhang, Prediction of convection-enhanced drug delivery to the human brain, Journal of Theoretical Biology, 250 (2008) 125-138.

[39] W. Zhan, C.-H. Wang, Convection enhanced delivery of liposome encapsulated doxorubicin for brain tumour therapy, Journal of Controlled Release, 285 (2018) 212-229.

[40] M. Kohandel, M. Kardar, M. Milosevic, S. Sivaloganathan, Dynamics of tumor growth and combination of anti-angiogenic and cytotoxic therapies, Physics in Medicine & Biology, 52 (2007) 3665-3677.

[41] S. Yonucu, D. Yılmaz, C. Phipps, M.B. Unlu, M. Kohandel, Quantifying the effects of antiangiogenic and chemotherapy drug combinations on drug delivery and treatment efficacy, PLoS computational biology, 13 (2017) e1005724.

[42] J.R. Less, T.C. Skalak, E.M. Sevick, R.K. Jain, Microvascular architecture in a mammary carcinoma: branching patterns and vessel dimensions, Cancer research, 51 (1991) 265-273.

[43] D.Y. Arifin, K.Y.T. Lee, C.-H. Wang, K.A. Smith, Role of convective flow in carmustine delivery to a brain tumor, Pharmaceutical research, 26 (2009) 2289-2302.

[44] W.M. Saltzman, M.L. Radomsky, Drugs released from polymers: diffusion and elimination in brain tissue, Chemical Engineering Science, 46 (1991) 2429-2444.

[45] A. Bhandari, A. Bansal, A. Singh, R.K. Gupta, N. Sinha, Comparison of transport of chemotherapeutic drugs in voxelized heterogeneous model of human brain tumor, Microvascular Research, 124 (2019) 76-90.

[46] S. Eikenberry, A tumor cord model for doxorubicin delivery and dose optimization in solid tumors, Theoretical Biology and Medical Modelling, 6 (2009) 16-35.

[47] M. Kohandel, C.A. Haselwandter, M. Kardar, S. Sengupta, S. Sivaloganathan, Quantitative model for efficient temporal targeting of tumor cells and neovasculature, Computational and mathematical methods in medicine, 2011 (2011) 790721.

[48] D. Barboriak, Data From RIDER_NEURO_MRI, The Cancer Imaging Archive, (2015).

[49] K. Clark, B. Vendt, K. Smith, J. Freymann, J. Kirby, P. Koppel, S. Moore, S. Phillips, D. Maffitt, M. Pringle, The Cancer Imaging Archive (TCIA): maintaining and operating a public information repository, Journal of digital imaging, 26 (2013) 1045-1057.

[50] S.M. Tolaney, Y. Boucher, D.G. Duda, J.D. Martin, G. Seano, M. Ancukiewicz, W.T. Barry, S. Goel, J. Lahdenrata, S.J. Isakoff, Role of vascular density and normalization in response to neoadjuvant bevacizumab and chemotherapy in breast cancer patients, Proceedings of the National Academy of Sciences, 112 (2015) 14325-14330.

[51] S. Kalyanasundaram, V. Calhoun, K. Leong, A finite element model for predicting the distribution of drugs delivered intracranially to the brain, American Journal of Physiology-Regulatory, Integrative and Comparative Physiology, 273 (1997) R1810-R1821.

[52] L.K. Fung, M. Shin, B. Tyler, H. Brem, W.M. Saltzman, Chemotherapeutic drugs released from polymers: distribution of 1, 3-bis (2-chloroethyl)-l-nitrosourea in the rat brain, Pharmaceutical research, 13 (1996) 671-682.

[53] D.W. Green, R.H. Perry, Perry's Chemical Engineers' Handbook/edición Don W. Green y Robert H. Perry, 1973.

[54] H. Kimelberg, Water homeostasis in the brain: basic concepts, Neuroscience, 129 (2004) 851-860.

[55] M. Sniegowski, N. Mandava, M.Y. Kahook, Sustained intraocular pressure elevation after intravitreal injection of bevacizumab and ranibizumab associated with trabeculitis, The open ophthalmology journal, 4 (2010) 28-29.

[56] S. Gao, J. Singh, Effect of oleic acid/ethanol and oleic acid/propylene glycol on the in vitro percutaneous absorption of 5-fluorouracil and tamoxifen and the macroscopic barrier property of porcine epidermis, International journal of pharmaceutics, 165 (1998) 45-55.

[57] J.E. Wolff, S. Berrak, S.E. Koontz Webb, M. Zhang, Nitrosourea efficacy in high-grade glioma: a survival gain analysis summarizing 504 cohorts with 24193 patients, Journal of neuro-oncology, 88 (2008) 57-63.

[58] D.K. Shah, B.S. Shin, J. Veith, K. Tóth, R.J. Bernacki, J.P. Balthasar, Use of an anti-vascular endothelial growth factor antibody in a pharmacokinetic strategy to increase the efficacy of

intraperitoneal chemotherapy, Journal of Pharmacology and Experimental Therapeutics, 329 (2009) 580-591.

[59] J. Mei, Y. Cheng, Y. Song, Y. Yang, F. Wang, Y. Liu, Z. Wang, Experimental study on targeted methotrexate delivery to the rabbit brain via magnetic resonance imaging–guided focused ultrasound, Journal of Ultrasound in Medicine, 28 (2009) 871-880.

[60] J. Chen, F. Zehtabi, J. Ouyang, J. Kong, W. Zhong, M.M. Xing, Reducible self-assembled micelles for enhanced intracellular delivery of doxorubicin, Journal of Materials Chemistry, 22 (2012) 7121-7129.

[61] F. Petrelli, K. Borgonovo, S. Barni, Targeted delivery for breast cancer therapy: the history of nanoparticle-albumin-bound paclitaxel, Expert opinion on pharmacotherapy, 11 (2010) 1413-1432.

[62] T.-L. Hwang, C.-L. Fang, C.-H. Chen, J.-Y. Fang, Permeation enhancer-containing water-in-oil nanoemulsions as carriers for intravesical cisplatin delivery, Pharmaceutical research, 26 (2009) 2314-2323.

[63] T. Formariz, V. Sarmento, A. Silva-Junior, M. Scarpa, C.V. Santilli, A. Oliveira, Doxorubicin biocompatible O/W microemulsion stabilized by mixed surfactant containing soya phosphatidylcholine, Colloids and Surfaces B: Biointerfaces, 51 (2006) 54-61.

[64] L.K. Fung, M.G. Ewend, A. Sills, E.P. Sipos, R. Thompson, M. Watts, O.M. Colvin, H. Brem, W.M. Saltzman, Pharmacokinetics of interstitial delivery of carmustine, 4-hydroperoxycyclophosphamide, and paclitaxel from a biodegradable polymer implant in the monkey brain, Cancer Research, 58 (1998) 672-684.

[65] D.S. Wishart, C. Knox, A.C. Guo, S. Shrivastava, M. Hassanali, P. Stothard, Z. Chang, J. Woolsey, DrugBank: a comprehensive resource for in silico drug discovery and exploration, Nucleic acids research, 34 (2006) D668-D672.

[66] W. Cole, W. Wolf, Preparation and metabolism of a cisplatin/serum protein complex, Chemico-biological interactions, 30 (1980) 223-235.

[67] M. Maia, S. Saivin, E. Chatelut, M. Malmary, G. Houin, In vitro and in vivo protein binding of methotrexate assessed by microdialysis, International journal of clinical pharmacology and therapeutics, 34 (1996) 335-341.

[68] R.F. Greene, J.M. Collins, J.F. Jenkins, J.L. Speyer, C.E. Myers, Plasma pharmacokinetics of adriamycin and adriamycinol: implications for the design of in vitro experiments and treatment protocols, Cancer research, 43 (1983) 3417-3421.

[69] H.-J. Kuh, S.H. Jang, M.G. Wientjes, J.L.-S. Au, Computational model of intracellular pharmacokinetics of paclitaxel, Journal of Pharmacology and Experimental Therapeutics, 293 (2000) 761-770.

[70] R.K. Jain, Transport of molecules in the tumor interstitium: a review, Cancer research, 47 (1987) 3039-3051.

[71] W. Zhan, W. Gedroyc, X.Y. Xu, Towards a multiphysics modelling framework for thermosensitive liposomal drug delivery to solid tumour combined with focused ultrasound hyperthermia, Biophysics Reports, 5 (2019) 43-59.

[72] Y.-M.F. Goh, H.L. Kong, C.-H. Wang, Simulation of the delivery of doxorubicin to hepatoma, Pharmaceutical Research, 18 (2001) 761-770.

[73] J.-F. Lu, R. Bruno, S. Eppler, W. Novotny, B. Lum, J. Gaudreault, Clinical pharmacokinetics of bevacizumab in patients with solid tumors, Cancer chemotherapy and pharmacology, 62 (2008) 779-786.

[74] A. Buur, H. Bundgaard, Prodrugs of 5-fluorouracil. III. Hydrolysis kinetics in aqueous solution and biological media, lipophilicity and solubility of various 1-carbamoyl derivatives of 5-fluorouracil, International journal of pharmaceutics, 23 (1985) 209-222.

[75] P.B. Layton, H.S. Greenberg, P.L. Stetson, W.D. Ensminger, J.W. Gyves, BCNU solubility and toxicity in the treatment of malignant astrocytomas, Journal of neurosurgery, 60 (1984) 1134-1137.

[76] W.-P. Liu, Q.-S. Ye, Y. Yu, X.-Z. Chen, S.-Q. Hou, L.-G. Lou, Y.-P. Yang, Y.-M. Wang, Q. Su, Novel lipophilic platinum (II) compounds of salicylate derivatives, Platinum Metals Review, 52 (2008) 163-171.

[77] I.V. Tetko, J. Gasteiger, R. Todeschini, A. Mauri, D. Livingstone, P. Ertl, V.A. Palyulin, E.V. Radchenko, N.S. Zefirov, A.S. Makarenko, Virtual computational chemistry laboratory–design and description, Journal of computer-aided molecular design, 19 (2005) 453-463.

[78] R.T. Liggins, W. Hunter, H.M. Burt, Solid-state characterization of paclitaxel, Journal of pharmaceutical sciences, 86 (1997) 1458-1463.

[79] C.M. Hand, J.R. Vender, P. Black, Chemotherapy in experimental brain tumor, part 1: in vitro colorimetric MTT assay, Journal of neuro-oncology, 36 (1998) 1-6.

[80] D.J. Kerr, A.M. Kerr, R.I. Freshney, S.B. Kaye, Comparative intracellular uptake of adriamycin and 4'-deoxydoxorubicin by nonsmall cell lung tumor cells in culture and its relationship to cell survival, Biochemical pharmacology, 35 (1986) 2817-2823.

[81] J.F. Gross, A.S. Popel, Mathematical models of transport phenomena in normal and neoplastic tissue, CRC Press, Boca Raton, FL, USA, 1979.

[82] C.G. Willett, Y. Boucher, E. Di Tomaso, D.G. Duda, L.L. Munn, R.T. Tong, D.C. Chung, D.V. Sahani, S.P. Kalva, S.V. Kozin, Direct evidence that the VEGF-specific antibody bevacizumab has antivascular effects in human rectal cancer, Nature medicine, 10 (2004) 145-147.

[83] H.S. Friedman, M.D. Prados, P.Y. Wen, T. Mikkelsen, D. Schiff, L.E. Abrey, W. Yung, N. Paleologos, M.K. Nicholas, R. Jensen, Bevacizumab alone and in combination with irinotecan in recurrent glioblastoma, J clin oncol, 27 (2009) 4733-4740.

[84] T.N. Kreisl, L. Kim, K. Moore, P. Duic, C. Royce, I. Stroud, N. Garren, M. Mackey, J.A. Butman, K. Camphausen, Phase II trial of single-agent bevacizumab followed by bevacizumab plus irinotecan at tumor progression in recurrent glioblastoma, Journal of clinical oncology, 27 (2009) 740-745.

[85] U. Bogdahn, P. Hau, G. Stockhammer, N. Venkataramana, A. Mahapatra, A.a. Suri, A. Balasubramaniam, S. Nair, V. Oliushine, V. Parfenov, Targeted therapy for high-grade glioma with the TGF-β2 inhibitor trabedersen: results of a randomized and controlled phase IIb study, Neuro-oncology, 13 (2010) 132-142.

[86] J. Voges, R. Reszka, A. Gossmann, C. Dittmar, R. Richter, G. Garlip, L. Kracht, H.H. Coenen, V. Sturm, K. Wienhard, Imaging-guided convection-enhanced delivery and gene therapy of glioblastoma, Annals of Neurology: Official Journal of the American Neurological Association and the Child Neurology Society, 54 (2003) 479-487.

[87] C. Liu, X.Y. Xu, A systematic study of temperature sensitive liposomal delivery of doxorubicin using a mathematical model, Computers in biology and medicine, 60 (2015) 107-116.

[88] W. Zhan, Delivery of liposome encapsulated temozolomide to brain tumour: Understanding the drug transport for optimisation, International journal of pharmaceutics, 557 (2019) 280-292.

[89] T. Tagami, M.J. Ernsting, S.-D. Li, Optimization of a novel and improved thermosensitive liposome formulated with DPPC and a Brij surfactant using a robust in vitro system, Journal of controlled release, 154 (2011) 290-297.

[90] C. Saraiva, C. Praça, R. Ferreira, T. Santos, L. Ferreira, L. Bernardino, Nanoparticle-mediated brain drug delivery: overcoming blood–brain barrier to treat neurodegenerative diseases, Journal of Controlled Release, 235 (2016) 34-47.

[91] A. Gaudin, E. Song, A.R. King, J.K. Saucier-Sawyer, R. Bindra, D. Desmaële, P. Couvreur, W.M. Saltzman, PEGylated squalenoyl-gemcitabine nanoparticles for the treatment of glioblastoma, Biomaterials, 105 (2016) 136-144.

[92] X. Fu, J. Cai, X. Zhang, W. Li, H. Ge, Y. Hu, Top-down Fabrication of Shape-controlled, Monodisperse Nanoparticles for Biomedical Applications, Advanced Drug Delivery Reviews, 132 (2018) 169-187.

[93] A.A. Linninger, M.R. Somayaji, L. Zhang, M.S. Hariharan, R.D. Penn, Rigorous mathematical modeling techniques for optimal delivery of macromolecules to the brain, IEEE Transactions on Biomedical Engineering, 55 (2008) 2303-2313.

[94] M. Inglesby, S. Zeronian, Diffusion coefficients for direct dyes in aqueous and polar aprotic solvents by the NMR pulsed-field gradient technique, Dyes and pigments, 50 (2001) 3-11.

[95] T.P. Butler, F.H. Grantham, P.M. Gullino, Bulk transfer of fluid in the interstitial compartment of mammary tumors, Cancer Research, 35 (1975) 3084-3088.

[96] K. Neeves, C. Lo, C. Foley, W. Saltzman, W. Olbricht, Fabrication and characterization of microfluidic probes for convection enhanced drug delivery, Journal of controlled release, 111 (2006) 252-262.

[97] M. Soltani, P. Chen, Effect of tumor shape and size on drug delivery to solid tumors, Journal of biological engineering, 6 (2012) 4-18.

[98] W. Zhan, W. Gedroyc, X.Y. Xu, Effect of heterogeneous microvasculature distribution on drug delivery to solid tumour, Journal of Physics D: Applied Physics, 47 (2014) 475401.

[99] A. Bhandari, A. Bansal, A. Singh, N. Sinha, Perfusion kinetics in human brain tumor with DCE-MRI derived model and CFD analysis, Journal of biomechanics, 59 (2017) 80-89.

[100] J. Zhao, H. Salmon, M. Sarntinoranont, Effect of heterogeneous vasculature on interstitial transport within a solid tumor, Microvascular research, 73 (2007) 224-236.

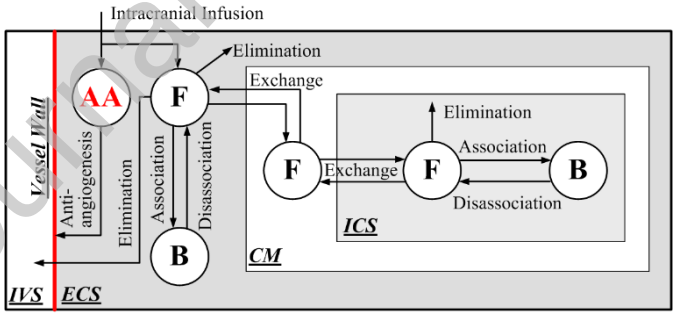

Figure 1. Schematic diagram of drug transport processes in CED, in which the letters of AA, F and B refer to *bevacizumab*, anticancer drugs in their free form and the drugs that binds with protein, respectively.

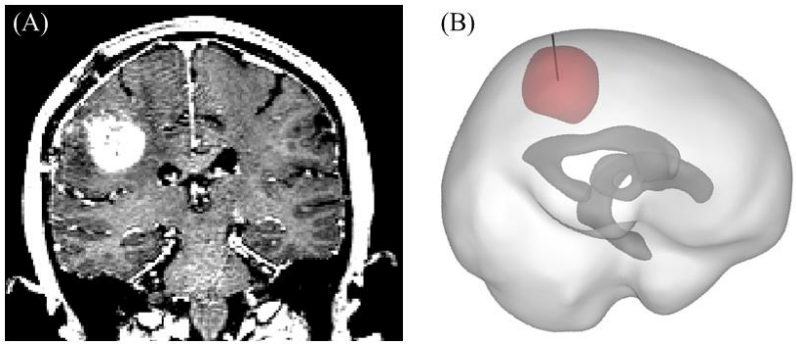

Figure 2. Model geometry. (A) A representative MR image slice, (B) reconstructed 3-D geometry. The brain tumour, ventricle and holding tissue are marked in red, dark grey and pale grey, respectively. A catheter in black is placed in the centre of tumour for drug release. The diameter of the catheter is 1 mm.

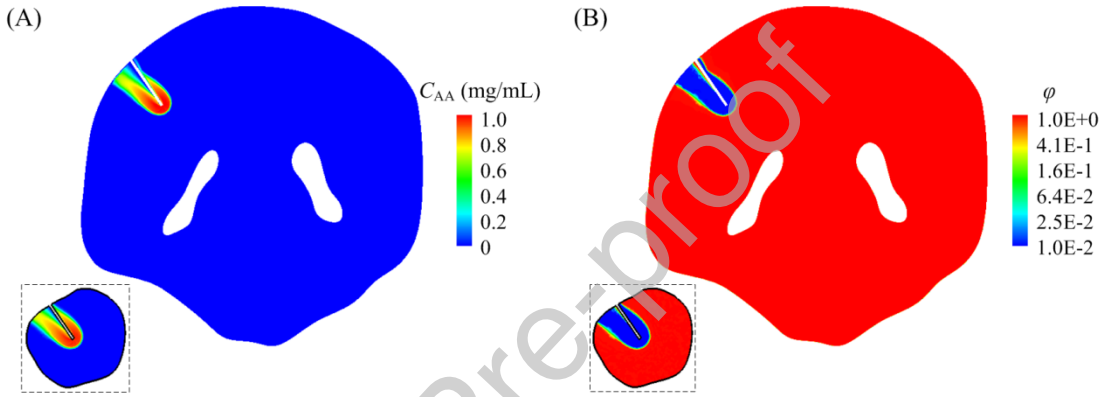

Figure 3. Spatial distribution of (A) *bevacizumab* and (B) variation scale of microvascular density, φ, on a cross section of the brain. The distribution of *bevacizumab* and φ within the brain tumour are highlighted in the dotted boxes in the left bottom corner of (A) and (B), respectively.

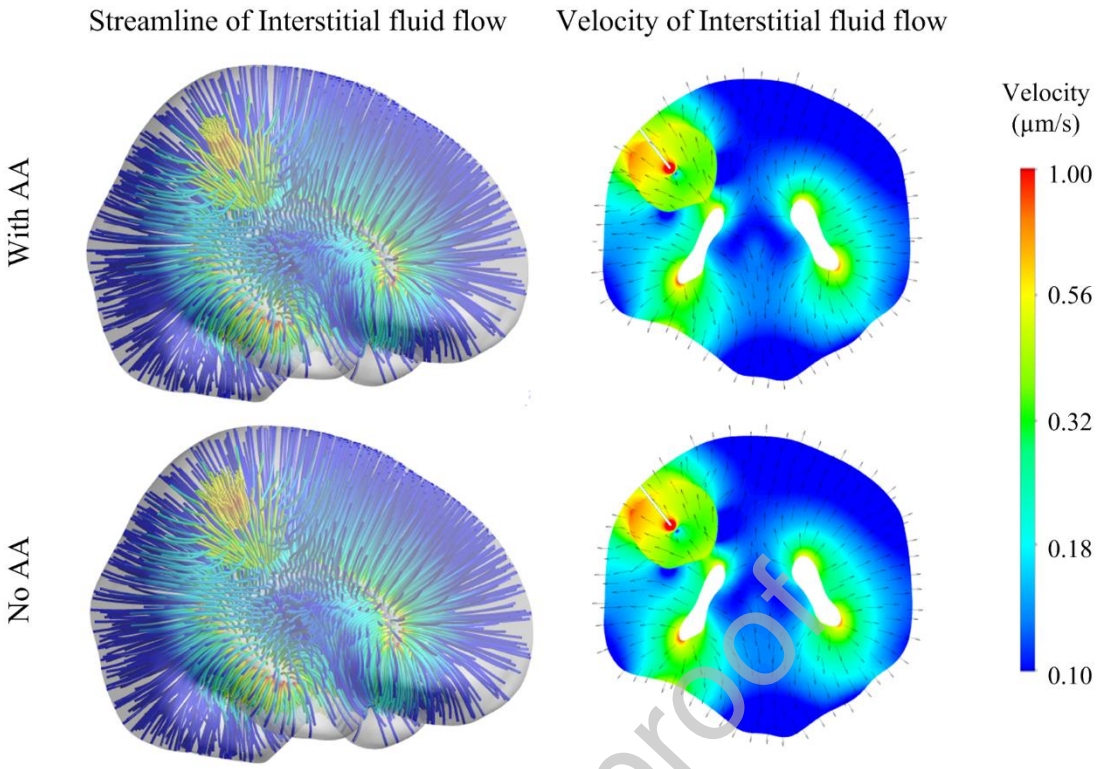

735

736 **Figure 4. The interstitial fluid flow in the entire brain in the treatment with and without *bevacizumab*.**
737 **The streamline of interstitial fluid flow is represented in 3D in the entire brain. The interstitial fluid**
738 **velocity is shown on a cross-section, with black arrows indicating the local flow direction.**

739

740

741

742

743

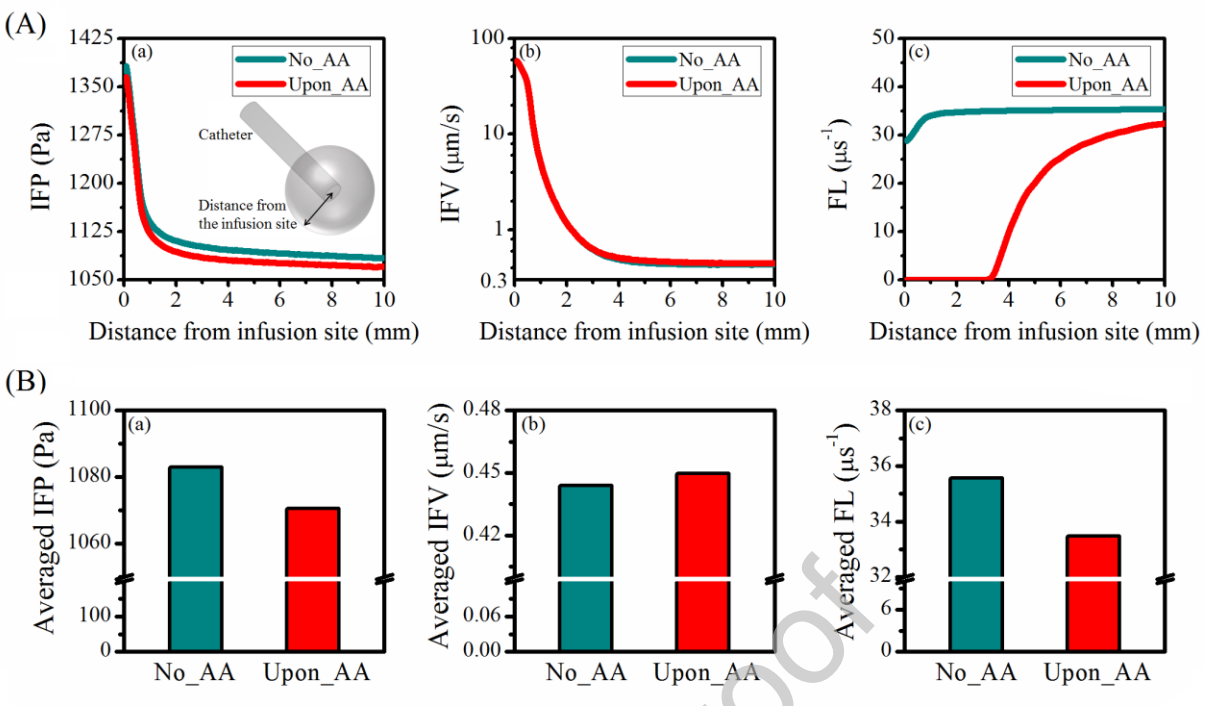

744
745

746 **Figure 5. Comparison of interstitial fluid flow in the treatments with and without *bevacizumab*. (a)**
747 **Interstitial fluid pressure, (b) velocity and (c) fluid leakage rate from blood are represented as a function**
748 **of distance from the infusion site in panel (A). The spatial averaged values in the entire tumour are given**
749 **in panel (B). The fluid loss rate from blood is determined by the transvascular pressure gradient and**
750 **microvasculature density, calculated by Eq. (2). Infusion rate is 3.0 μL/min.**

751

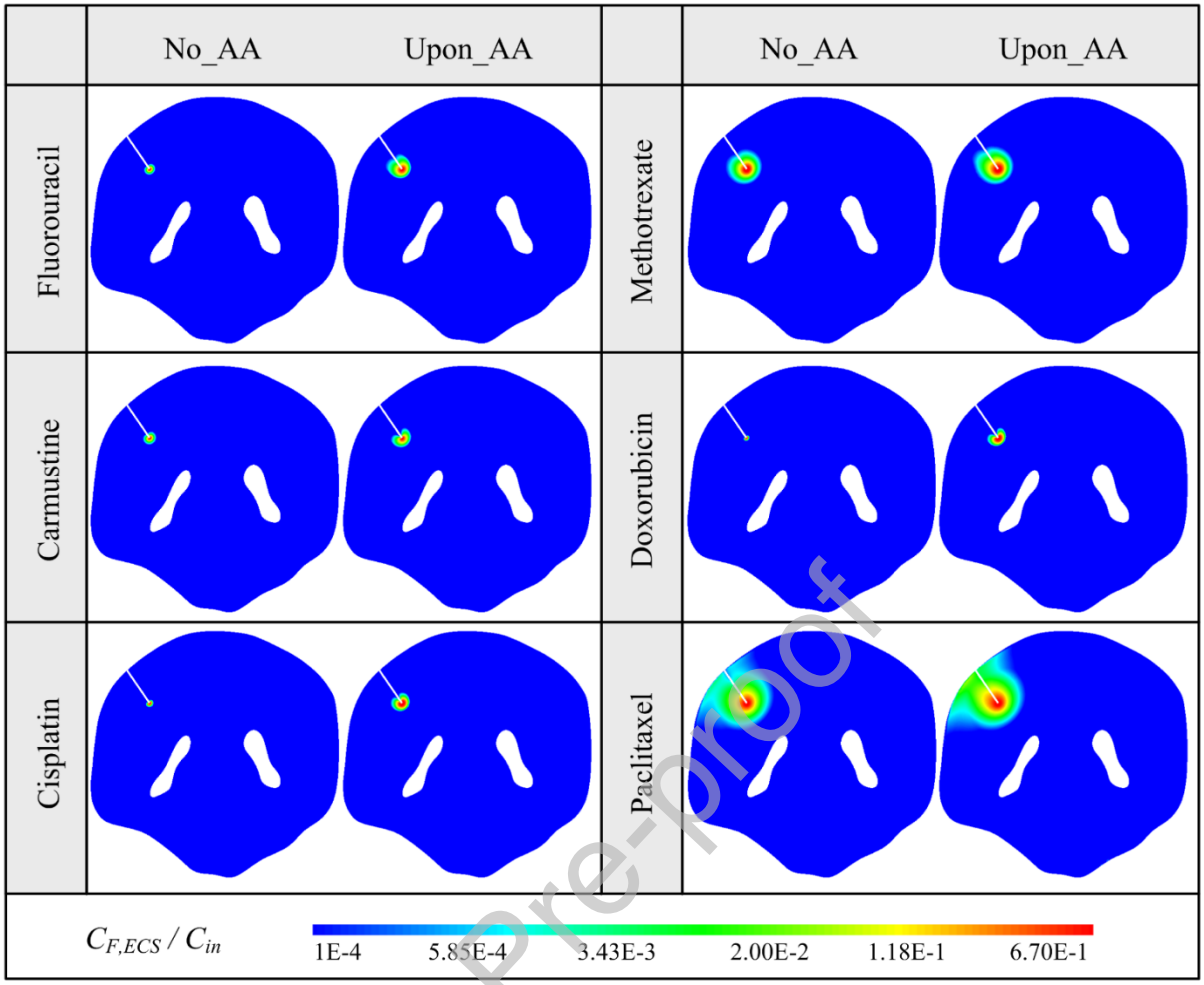

752

753 **Figure 6. Comparison of drug spatial distribution in the treatments with and without *bevacizumab* on a**
754 **cross section of the brain.**

755

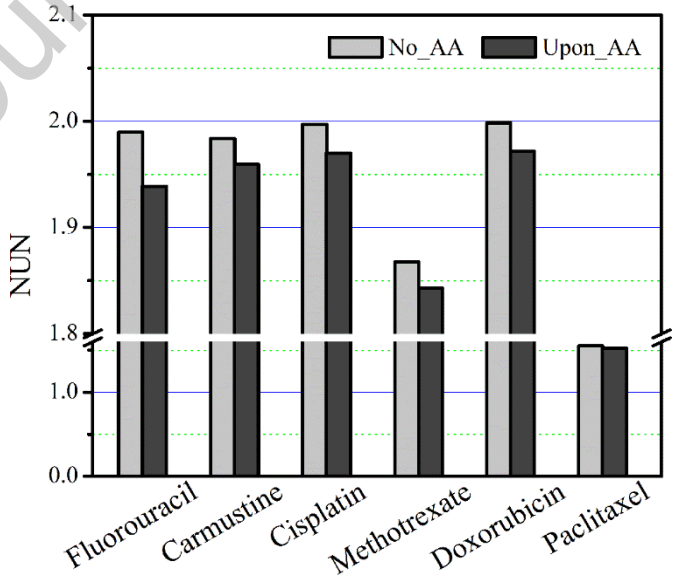

756

757 **Figure 7. Non-uniformity (NUN) of drug spatial distribution in the treatment with and without**
758 ***bevacizumab*.**

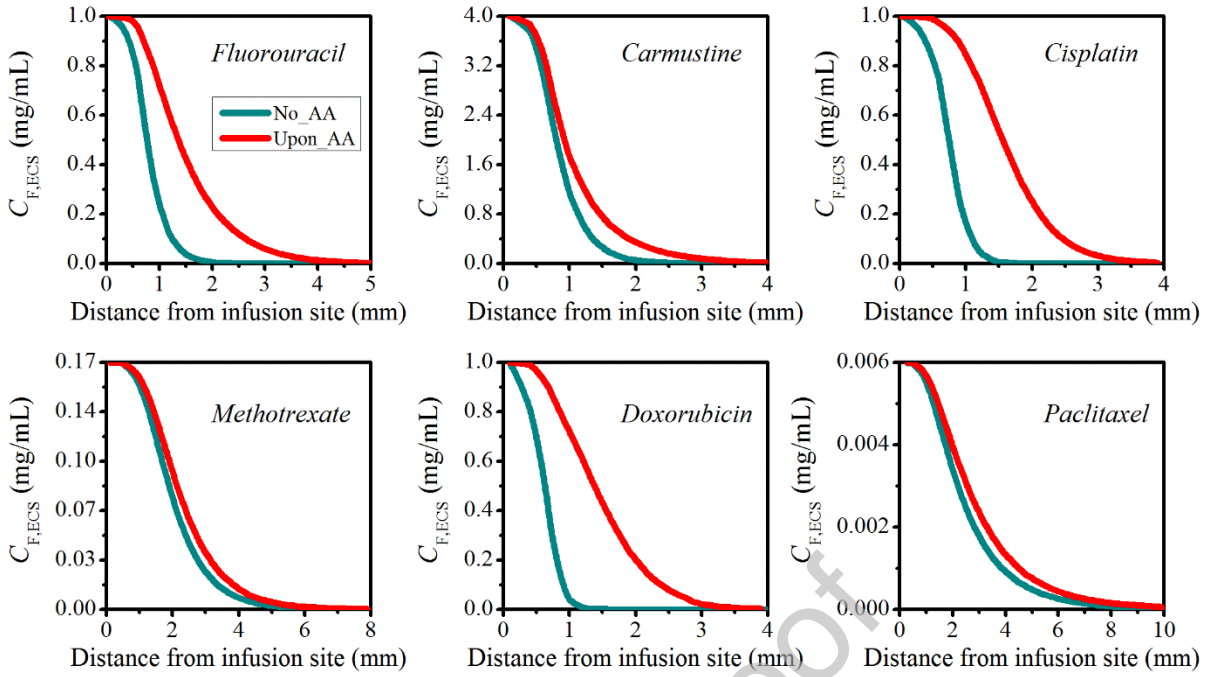

759

760 **Figure 8. Comparison of cytotoxic drug concentrations in the CED treatment with and without**
761 ***bevacizumab*. Volume averaged ECS concentration of each drug is represented as a function of the**
762 **distance from infusion site. Infusion rate is 3.0 μL/min.**

763

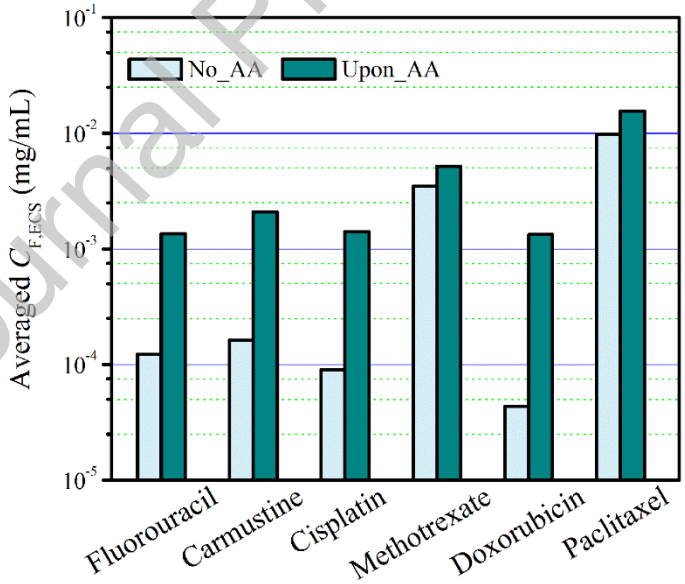

764

765 **Figure 9. Comparison of spatial averaged concentration (C_{avg})) of each cytotoxic drugs in the treatment**
766 **with and without *bevacizumab*.**

767

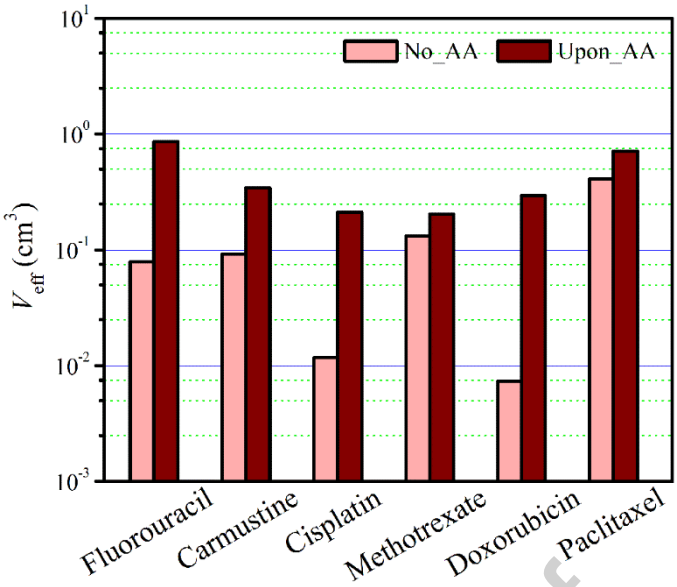

Figure 10. Comparison of effective distribution volume (V_{eff}) of each cytotoxic drugs in the treatment with and without *bevacizumab*.

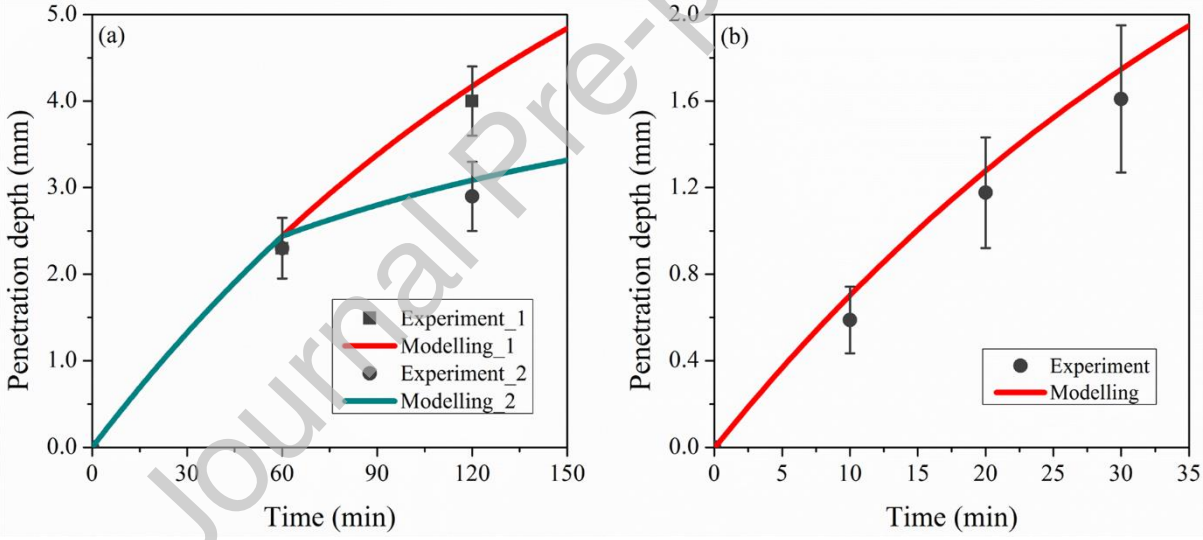

Figure 11. Comparison of modelling predictions and experimental data on the penetration depth of trypan blue upon CED infusion. (a) presents the results of two delivery strategies using a 30G needle. Trypan blue is continuously infused into gel at the rate 0.5μL/min for 120min in Experiment_1, whereas, the continuous infusion at the same rate only lasts for 60min in Experiment_2. (b) shows the results of infusing trypan blue at the rate 1.0μL/min through a 27G needle. The experimental data of (a) and (b) is extracted from Ref. [93] and [38], respectively, with the diffusivity of trypan blue 3.0E-9 m^2/s adopted [38, 94]. There are good agreements of predicted penetration depths within the experimental measurement errors.

783 **Table 1. Biological properties of tumour and surrounding tissue**

Symbol	Parameter	Brain Tumour	Normal Tissue
υ_{ECS}	Volume fraction of extracellular space	0.35 [51]	0.20 [52]
υ_{ICS}	Volume fraction of intracellular space	0.55 [51]	0.65 [52]
α	Angiogenesis parameter (s^{-1})	-1.85E-6 [47]	-1.85E-6 [47]
β	Angiogenesis parameter (s^{-1})	5.56E-6 [47]	5.56E-6 [47]
γ	Angiogenesis parameter (s^{-1})	-3.71E-6 [47]	-3.71E-6 [47]
ρ	Density of interstitial fluid (kg/m^3)	1000 [53]	1000 [53]
μ	Viscosity of interstitial fluid (kg/m/s)	7.8E-4 [53]	7.8E-4 [53]
π_b	Osmotic pressure of blood (Pa)	3440 [54]	3440 [54]
π_i	Osmotic pressure of interstitial fluid (Pa)	1110 [34]	740 [34]
p_b	Pressure of blood in microvasculature (Pa)	4610 [54]	4610 [54]
S/V	Initial Ratio of vessel surface area over tissue volume (m^{-1})	20000 [34]	7000 [34]
σ_T	Osmotic reflection coefficient for blood proteins	0.82 [34]	0.91 [34]
K_b	Hydraulic conductivity of the vessel wall (m/Pa/s)	1.1E-12 [43]	1.4E-13 [43]
κ	Darcian permeability (m^2)	6.4E-14 [43]	6.5E-15 [43]

784

785

786 **Table 2. Transport properties of anti-angiogenetic and anti-cancer agents**

Symbol	Parameter	Bevacizumab	Fluorouracil	Carmustine	Cisplatin	Methotrexate	Doxorubicin	Paclitaxel
MW	Molecular weight (g/mol)	1.49E5 [55]	130.08 [56]	214.05 [57]	300.01 [58]	454.44 [59]	543.52 [60]	853.91 [61]
$P_{ICS\text{-}ECS}$	Partition coefficient between ICS and ECS	-	1.0 [52]	1.0 [52]	1.0 [52]	1.0 [52]	1.0 [52]	1.0 [52]
$P_{CM\text{-}ECS}$	Partition coefficient between CM and ECS	-	0.1 [44]	10.3 [52]	0.006 [62]	0.01 [44]	0.3 [63]	3162.3 [64]
K_{ECS}, K_{ICS}	Binding constant between free and bound drugs in ECS and ICS	-	0.1 [65]	5.0 [52]	1.0 [66]	0.7 [67]	3.0 [68]	5.1 [69]
D_{ECS}	Diffusion coefficient in ECS (m^2/s)	3.2E-12 [70]	1.2E-9 [44]	1.5E-9 [52]	2.5E-10 [58]	5.3E-10 [44]	3.4E-10 [71]	9.0E-10 [64]
P	Transvascular permeability (m/s)	-	9.0E-7 [44]	7.0E-7 [52]	1.5E-6 [58]	1.4E-8 [44]	3.0E-6 [71]	7.0E-9 [64]
k_e	Drug elimination due to reactions (s^{-1})	1.2E-5 [47]	5.6E-4 [44]	1.1E-4 [52]	7.3E-4 [58]	1.5E-4 [44]	5.8E-4 [72]	6.8E-7 [64]
k_{AK}	Anti-angiogenetic rate (s^{-1})	2.0E-6 [50]	-	-	-	-	-	-
C_{in}	Infusion solution concentration (M)	6.7E-4 [73]	7.7E-3 [74]	1.9E-2 [75]	3.3E-3 [76]	3.7E-4 [77]	1.84E-3 [77]	7.0E-6 [78]
LD90	Effective therapeutic concentration (M)	-	2.0E-6 [79]	1.5E-5 [64]	2.0E-5 [79]	5.9E-5 [79]	2.39E-6 [80]	8.9E-7 [64]

787

788

789 **Table 3. Relative importance of convective transport of each cytotoxic drug in brain tumour.**

	Fluorouracil	Carmustine	Cisplatin	Methotrexate	Doxorubicin	Paclitaxel
No_AA	0.26	1.76	0.82	3.05	1.01	872.76
Upon_AA	0.27	1.84	0.86	3.13	1.05	912.11

790

791

792 **Table 4. Relative importance of microvascular-related elimination of each cytotoxic drug in brain tumour.**

	Fluorouracil	Carmustine	Cisplatin	Methotrexate	Doxorubicin	Paclitaxel
No_AA	3.94E-06	6.03E-07	8.26E-06	2.22E-08	1.36E-05	6.38E-11
Upon_AA	3.68E-06	5.64E-07	7.72E-06	2.08E-08	1.27E-05	5.99E-11

793

794

795 **Table 5. Karlovitz number of each cytotoxic drugs in brain tumour.**

	Fluorouracil	Carmustine	Cisplatin	Methotrexate	Doxorubicin	Paclitaxel
No_AA	3.61E-03	4.90E-03	2.27E-03	9.19E-02	1.14E-03	2.90E-01
Upon_AA	3.89E-03	5.30E-03	2.46E-03	9.61E-02	1.24E-03	3.13E-01

796

797